

# Impact of mesoscale eddies on water transport between the Pacific Ocean and the Bering Sea

S.V. Prants, A.A. Andreev, M.V. Budyansky, and M.Yu. Uleysky  
*Pacific Oceanological Institute of the Russian Academy of Sciences,  
43 Baltiiskaya st., 690041 Vladivostok, Russia\**

Sea surface height anomalies observed by satellites in 1993–2012 are combined with simulation and observations by surface drifters and Argo floats to study water flow pattern in the Near Strait (NS) connected the Pacific Ocean with the Bering Sea. Daily Lagrangian latitudinal maps, computed with the AVISO surface velocity field, and calculation of the transport across the strait show that the flow through the NS is highly variable and controlled by mesoscale and submesoscale eddies in the area. On the seasonal scale, the flux through the western part of the NR is negatively correlated with the flux through its eastern part ( $r = -0.93$ ). On the interannual time scale, a significant positive correlation ( $r = 0.72$ ) is diagnosed between the NS transport and the wind stress in winter. Increased southward component of the wind stress decreases the northward water transport through the strait. Positive wind stress curl over the strait area in winter–spring generates the cyclonic circulation and thereby enhances the southward flow in the western part ( $r = -0.68$ ) and northward flow in the eastern part ( $r = 0.61$ ) of the NR. In fall, the water transport in different parts of the NS is determined by the strength of the anticyclonic mesoscale eddy located in the Alaskan Stream area.

Keywords: Transport across the Near Strait, mesoscale eddy dynamics, Lagrangian latitudinal maps

---

\* <http://dynalab.poi.dvo.ru>; [prants@poi.dvo.ru](mailto:prants@poi.dvo.ru)

## I. INTRODUCTION

Circulation in the Bering Sea is strongly influenced by the Alaskan Stream, which enters the Bering Sea through the many passes in the Aleutian Arc. The Aleutian Arc forms a porous boundary between the Bering Sea and the North Pacific. The inflow into the Bering Sea is balanced by outflow through the Kamchatka Strait, so that circulation in the Bering Sea basin may be described as a continuation of the North Pacific subarctic gyre (Fig. 1). Most of the transport into the Bering Sea occurs through the Near Strait ( $6\text{--}12 \times 10^6 \text{ m}^3/\text{s}$ ). The NS with its maximum depth of 1600 m, averaged depth of 650 m and width of 360 km is located between the Komandorsky Islands and the Attu Island (Near Islands). The existence of the Stalemate Bank (near  $53^\circ\text{N}$ ,  $171^\circ\text{E}$ ), with depths  $< 100 \text{ m}$ , in the eastern deep part of the NS may lead to topographically-induced dynamics in strait flows. Recent studies (current mooring measurements and model simulations) indicate that the flow through the NS, as through the other Aleutian passes, is extremely variable [1–4]. Occasionally, instabilities (eddies) occur in the Alaskan Stream that inhibit flow into the Bering Sea through the NS [5]. The data from current moorings demonstrated that the inflow through the NS is not to be bounded and may migrate laterally [5]. Ezer and Oey [2] stated that the NS (“wide passage”), does not have well organized currents, but they are largely influenced by the mesoscale eddies that propagated across the strait. Based on modeling results, Kinney and Maslowski [3] concluded that the interannual variability in mass transport and property fluxes is particularly strong across the western Aleutian Island Passes, including the NS. Much of this variability can be attributed to the presence of meanders and eddies found both to the north and south of the passes, which are found to directly cause periodic flow reversals and maxima in the western passes. Panteleev [4] combined the sea surface height anomalies (observed by satellites in 1992–2010) with monthly climatology of temperature and salinity to estimate circulation in the southern Bering Sea. On the interannual time scale, significant negative correlation ( $r = -0.84$ ) was diagnosed between the NS transport and the Alaskan Stream. In particular, the NS inflow amplifies when the upstream Alaskan Stream is relatively weak, resulting in stronger recirculation in the western Bering Sea. Stronger Alaskan Stream appears to reduce the NS inflow and at the same time produces larger transport through the Aleutian Arc, which amplifies the main cyclonic gyre controlled by the continental slope within the Bering Slope Current region [4].

The Alaskan Stream carries relatively warm subsurface waters. Eddies in the Alaskan Stream along the Aleutian Islands could have a significant impact on the heat, freshwater, nutrient, and biota exchange between the coastal area to the south of the Aleutian Islands and the offshore region in the western and central subarctic North Pacific. In addition, eddies to the south of the Aleutian Islands were suggested to drive the flow between the North Pacific and the Bering Sea [6]. The effect of continued disruption of inflow to the Bering Sea would be an appreciable cooling ( $0.5^\circ\text{C}$ ) of subsurface waters [7]. These substantial changes in seawater temperature would affect the climate and ecosystem of the Bering Sea.

The goal of the paper is two-fold. Firstly, we use the NS as a case study to understand general characteristics of the strait dynamics. The second aim is to shed light on impact of mesoscale eddies on the water flux between the North Pacific and the Bering Sea.

We work in the framework of the Lagrangian approach to study transport at the sea surface in which one follows fluid particle trajectories in a velocity field calculated from altimetric measurements or obtained as an output of one of the ocean circulation models. The Lagrangian approach has been successfully applied to study large-scale mixing and transport in different seas and oceans (see, for example, Refs. [8–21] and references therein). In these papers methods, borrowed from dynamical systems theory, have been used to find hidden geometric structures in the ocean that organize complicated large-scale flows. Ones of the most important among them are Lagrangian coherent structures which are proxies of so-called stable and unstable manifolds of hyperbolic trajectories of fluid particles. Hyperbolicity is a concept in dynamical systems theory (for a review on application of that theory in physical oceanography see [11, 22]). It is characterized by the presence of expanding and contracting directions in the phase space of a dynamical system. This is a situation where phase trajectories converge in one direction and diverge in the other one. A hyperbolic stagnation point in a stationary system has stable and unstable manifolds along which the phase points approach it and move away from it, respectively. Typically, under a perturbation, a hyperbolic stagnation point of the unperturbed system becomes a hyperbolic trajectory,  $\gamma(t)$ , with stable,  $W_s(\gamma)$ , and unstable  $W_u(\gamma)$  invariant manifolds. In the enlarged phase space those manifolds are surfaces which do not coincide but intersect each other. A blob of the phase fluid in the phase space experiences stretching and folding that typically gives rise to chaotic motions even in purely deterministic dynamical systems, the remarkable phenomenon known as deterministic or dynamical chaos. The ultimate reason of that chaos is the instability of trajectories that is expressed in terms of the hyperbolicity conditions.

In fluid flows invariant manifolds are material surfaces composing of the same fluid particles in the course of time. In 2D fluid flows stable and unstable manifolds of a hyperbolic trajectory  $\gamma(t)$  are material lines consisting of a set of points through which at time moment  $t$  pass trajectories asymptotically to  $\gamma(t)$  at  $t \rightarrow \infty$  ( $W_s$ ) and  $t \rightarrow -\infty$  ( $W_u$ ) [11, 22]. They are complicated curves infinite in time and space that act as boundaries to fluid transport.

Theory of chaotic motions, known as chaotic advection [23], is well developed in time periodic 2D flows where periodic hyperbolic trajectories can be seen as fixed points using Poincaré maps. The stable and unstable manifolds of hyperbolic trajectories can be computed using different techniques and are known to form complex homoclinic or heteroclinic tangles which are “seeds” of chaotic advection.

There is a commonly used method for detecting stable and unstable manifolds in irregular and even turbulent flows based on computing Lyapunov exponents where a region under study is seeded with a large number of tracers for each of which the finite-time Lyapunov exponents are computed forward and backward in time. The curves of local maxima (ridges) in the Lyapunov scalar field, attributed to initial tracer’s positions, approximate stable manifolds when solving equations of motion forward in time and unstable ones when solving them backward in time [9, 10, 13, 14, 16, 21].

We apply the Lagrangian approach to model transport through the NS and compute trajectories of a large number of synthetic tracers advected by the interpolated AVISO geostrophic velocity field. Our main goal is to study not mixing but transport through the NS that can be characterized more adequately by computing not the Lyapunov exponents but the other Lagrangian indicators that have been recently introduced in [16, 20, 21, 24]. In the context of this paper, the most appropriate among them are meridional displacements of tracers that are computed after solving the advection equations backward in time in an interpolated altimetric velocity field. As the result, we get daily synoptic latitudinal maps around the NS that show clearly not only mesoscale and submesoscale eddies in the region but as well origin and history of waters crossing the strait for a given period of time.

The paper is organized as follows. Section 2 details the data and methods used in the paper. Section 3 contains the main results. We consider typical hydrological situations in different seasons and years with various types of eddies to be present in the strait and around it. The representative latitudinal synoptic maps demonstrate clearly those eddies and provide us with information about the direction of transport through different parts of the strait and its dependence on the number and polarity of the eddies. The daily transport across different parts of the strait has been calculated in 1993–2012 to show that the flow is highly variable and controlled by mesoscale and submesoscale eddies in the area. The section is ended with establishing a correlation between the NS transport and the wind stress.

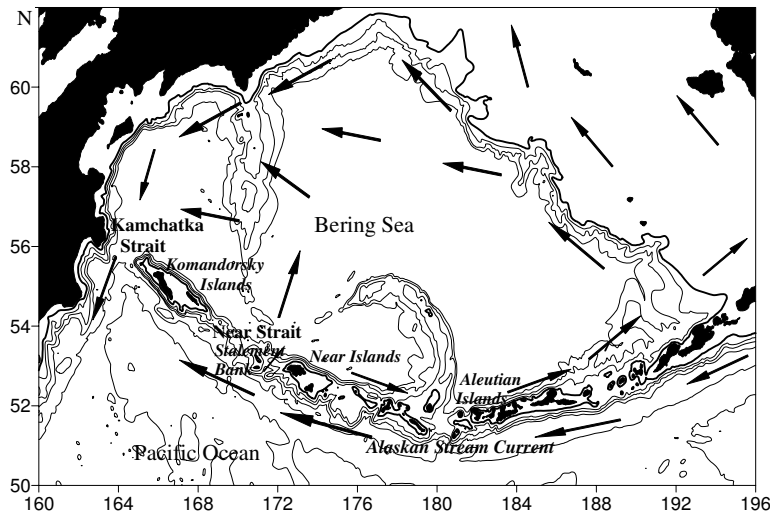


FIG. 1. Schematic representation of the currents in the northern North Pacific and the Bering Sea.

## II. DATA AND METHODS

Since 1992, the ocean surface topography has been continuously observed from space by the Topex/Poseidon, European Remote Sensing (ERS), Geosat Follow-On (GFO), Envisat and Jason satellite missions. These data are available at <http://www.aviso.oceanobs.com>. We use the gridded sea surface height anomalies (SSHA) for the period of 1993–2012 for the diagnostic computations. For each 7-day period, the SSHAs, obtained by optimal interpolation of all the available altimeter missions, were downloaded from the Aviso site.

Geostrophic velocities were obtained from the AVISO database. The data is gridded on a  $1/3^\circ \times 1/3^\circ$  Mercator grid. Geostrophic velocities were calculated from the sea-surface height anomalies by solving the equation for geostrophic equilibrium. Bicubic spatial interpolation and third order Lagrangian polynomials in time have been used to provide

accurate numerical results. Lagrangian trajectories have been computed by integrating the advection equations with a fourth-order Runge-Kutta scheme with a fixed time step of 0.001th part of a day.

Motion of a fluid particle in a two-dimensional flow is the trajectory of a dynamical system with given initial conditions governed by the velocity field. The corresponding advection equations are written as follows:

$$\frac{dx}{dt} = u(x, y, t), \quad \frac{dy}{dt} = v(x, y, t), \quad (1)$$

where the longitude,  $x$ , and the latitude,  $y$ , of a passive particle are in geographical minutes,  $u$  and  $v$  are angular zonal and meridional components of the surface velocity expressed in minutes per day.

Drifter data were used in the study for validation purposes and consisted of two major components: surface drifters and subsurface Argo buoys. In this study, we use the monthly wind stress dataset from the NCEP reanalysis [25]. The horizontal resolution of the NCEP data is  $1.9^\circ \text{ lat} \times 1.8^\circ \text{ lon}$ .

Some of our conclusions are based on locating eddies on the Lagrangian synoptic latitudinal maps computed with the help of the altimetric geostrophic velocity field. The boundaries of the eddies are, as a rule, surrounded by the stable and unstable invariant manifolds of hyperbolic trajectories located nearby. Those structures to be computed at the ocean surface are determined mainly by the large-scale advection field which is appropriately captured by altimetry. The question is how robust are those Lagrangian features to inevitable errors in altimetric velocity fields. That problem has been carefully studied in literature. It has been shown theoretically [8] that the strong stable and unstable manifolds, existing for a sufficient long time, are robust to errors in observational or model velocity fields because the particle trajectories will in general diverge exponentially from the true trajectories near a stable manifold. The very manifolds are not expected to be perturbed to the same degree, because errors in the particle trajectories spread along them. They were found to be relatively insensitive to both sparse spatial and temporal resolution and to the velocity field interpolation method [15, 17, 18]. In particular, the method for locating boundaries of large eddies (more than 20 km in diameter) and strong jets with the help of Lyapunov exponents has been shown to be reliable [9, 10, 13, 14, 16, 20, 21]. However, small Lagrangian features are not well resolved from altimetry and should be considered with some caution. The comparison of the Lagrangian coherent structures computed with altimetric velocity fields in numerous paper (see, for example, [9, 12, 14, 19, 26]) with independent satellite and in situ measurements of thermal and other fronts in different seas and oceans has been shown a good correspondence.

### III. RESULTS AND DISCUSSION

#### A. Calculation of the water transport across the Near Strait

The width of the NS is sufficient (greater than the internal Rossby radius  $\sim 10\text{--}20$  km) to provide a northward flow on the east side and a southward flow on the west side. The relative strength of these two branches determines the direction and magnitude of the net transport in the NS that has been computed as follows. The line, crossing the strait from  $168.5^\circ\text{E}$ ,  $54.5^\circ\text{N}$  to  $172.3^\circ\text{E}$ ,  $53^\circ\text{N}$ , consists of 20 segments with 100 particles to be placed at each segment. The daily transport across each segment may be obtained by integrating velocity normal at a given point across the segment length. The northward (southward) transport is supposed to be positive (negative).

Fig. 2a shows that during the study period (1993–2012 yrs) the surface northward flow was enhanced in the central and eastern parts of the strait but the southward flow in the western side of strait was weak. The net transport through the NS was directed from the North Pacific to the Bering Sea. The transport time series through the western and eastern NS are negatively correlated (at the 99% significance level) (Fig. 2b). The correlation coefficient is  $-0.93$  for the monthly mean values. The correlation essentially means that when the inflow into the Bering Sea via the eastern NS is strong, the outflow via the western NS tends to be weak or southward. There is seasonality in the water flux through the NS. The northward water transport through the central and eastern parts of the NS is strong between March and June and relatively weak in August–October. The year-to-year change of the annually averaged volume transport through the NS is significantly correlated with the meridional wind stress ( $\tau_y$ , November–March) (Fig. 2c). An increase of southward component of the wind stress (positive values of  $\tau_y$ ) decreases the northward water flux through the strait ( $r = -0.72$ , 1997–2012).

#### B. Lagrangian synoptic maps

The satellite altimetry records and buoy and drifter tracks demonstrate that anticyclonic and cyclonic eddies to the north and south of the NS have been regularly observed. Synoptic latitudinal maps (Fig. 3) demonstrate the eddies and the origin of waters in study area during Summer–Fall 2003. All the maps have been computed by integrating

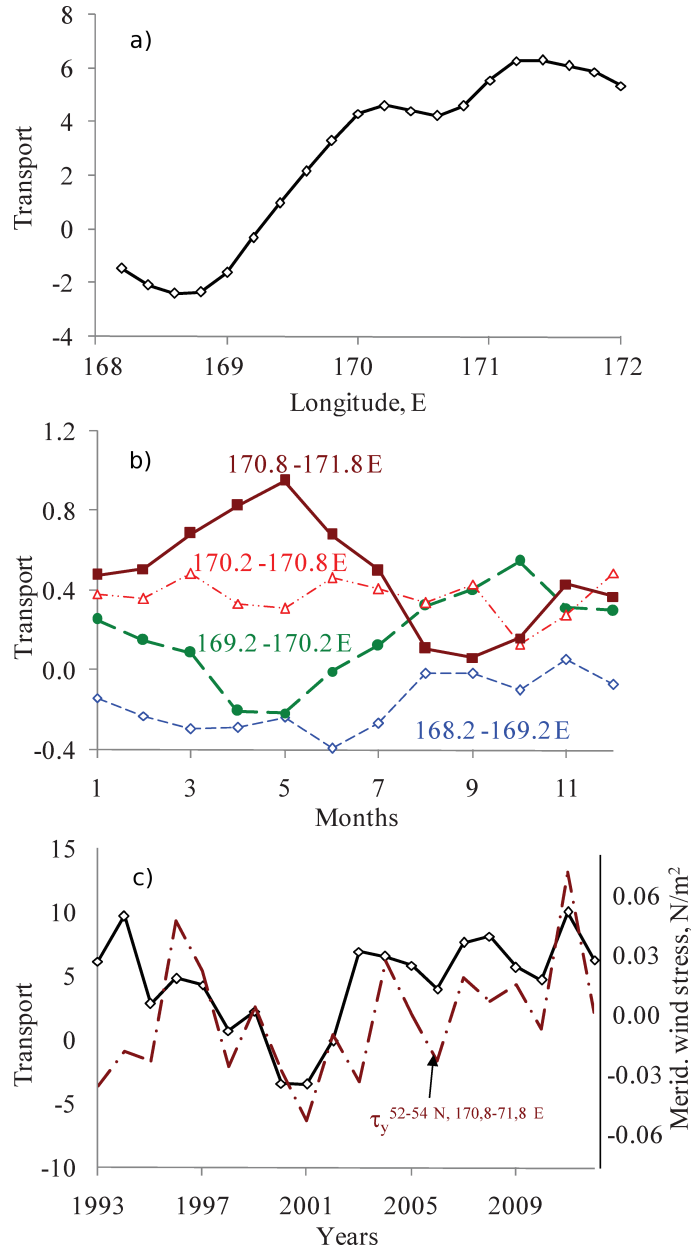


FIG. 2. Annually averaged water transport in the NS versus longitude (a); monthly averaged water transport in different parts of the NS (b) and the year-to-year changes of the water transport in the NS and the meridional wind stress (Nov.–Mar.) in the NS area (c).

the advection equations (1) for a large number of particles backward in time for 90 days before the date indicated on the corresponding map and coding by color the latitudes from which the corresponding particles came to their final positions on the map. Such maps provide information on the advection of waters through the strait in the meridional direction.

We mark “instantaneous” hyperbolic and elliptic stagnation points on the overlaid AVISO velocity field by crosses and circles, respectively. The elliptic points are usually situated in the centers of eddies and gyres. It is well known that besides “trivial” elliptic points, the motion around which is stable, there are hyperbolic points which organize fluid motion in their neighbourhood in a specific way. In a steady flow the hyperbolic points are typically connected by the separatrices which are their stable and unstable invariant manifolds. In a time-periodic flow the hyperbolic points are replaced by the corresponding hyperbolic trajectories with associated invariant manifolds which in general intersect transversally resulting in a complex manifold structure known as heteroclinic tangles. The fluid motion in

these regions is so complicated that it may be strictly called chaotic, the phenomenon known as chaotic advection (for a review see [11, 23, 27]). Adjacent fluid particles in such tangles rapidly diverge providing very effective mechanism for water mixing.

Firstly, we focus at the anticyclonic eddy that was tracked in the Alaskan Stream area south of the NS in the Spring-Fall 2003 (Fig. 3a). The elliptic point (dark circle) is situated in its center around  $x_0 = 171^\circ 30'E$ ,  $y_0 = 52^\circ 15'N$ . Dark grey and black colors on the latitudinal maps mean that the corresponding particles came to their positions for 90 days from the latitudinal to the north of the strait ( $> 53^\circ 54'N$ ), whereas the light grey and white colors mean that the corresponding particles came from the latitudinal to the south of the strait ( $< 53^\circ 54'N$ ). It had an elliptical shape with a dimension of  $120 \times 150$  km, and its center was located over the axis of the Aleutian bottom trench. According to the altimetry data, the eddy was formed in March–April 2003 to the southeastward of the Near Islands ( $\sim 173^\circ E$ ). In June 2003 it occupied the position to the south of the NS. The Lagrangian maps computed for May–July show that the northward transport prevails in the central and eastern parts of the NS (see “white” and “yellow” tongues in the printed and web versions of Fig. 3a, respectively).

The interaction of the mesoscale eddy with the Stalement Bank led to formation of the submesoscale topographic anticyclonic eddy (horizontal dimension of  $30 \times 40$  km) to the north of the bank in early August 2003. The elliptic point of that eddy is situated in its center around  $x_0 = 171^\circ E$ ,  $y_0 = 53^\circ 30'N$  (Fig. 3b). By the beginning of September, that submesoscale eddy was interacting with the mesoscale eddies to the north and south of the NS forming the triple vortex structure with two hyperbolic points (crosses) between the eddies and three elliptic ones in their centers (Fig. 3c). This structure changed significantly the character of transport, enhancing the northward flux through the central part of the NS and southward flux on the eastern side of the NS in August–September 2003. That result has been confirmed by direct calculation of daily and monthly fluxes in different parts of the NS. The grey filaments around the periphery of the eddies in that structure mark the waters that crossed for 90 days the eastern side of the NS from the north to the south. In the language of dynamical systems theory, the corresponding fluid particles were moving along the unstable manifolds of the hyperbolic points between the eddies that can be visualized approximately by computing the backward-in-time finite time Lyapunov exponents. By the end of September, the topographic eddy over the bank disappeared under the pitchfork bifurcation that opened a way to a northward flux through the central and eastern parts of the NS (Fig. 3d). Instead of that, one can see in Fig. 3d a pair of anticyclones to be formed in October to the south of the NS with a hyperbolic point between them.

We have checked our results shown in the latitudinal maps (Fig. 3) by computing the finite-time Lyapunov exponents using the method of the singular-value decomposition of an evolution matrix for the linearized advection equations proposed in [16]. This quantity characterizes asymptotically the average rate of the particle’s dispersion and is given by formulae

$$\lambda(t, t_0) = \frac{\ln \sigma(t, t_0)}{t - t_0}, \quad (2)$$

which is the ratio of the logarithm of the maximal possible stretching in a given direction to a time interval  $t - t_0$ . Here  $\sigma(t, t_0)$  is the maximal singular value of the evolution matrix. The Lyapunov field characterizes quantitatively mixing along with directions of maximal stretching and contracting, and it is applied to identify Lagrangian coherent structures in irregular velocity fields. In Fig. 4a and b we show two Lyapunov maps on the same days as in panels c and d in Fig. 3, respectively. The values of  $\lambda$  have been computed by integrating the advection equations (1) backward in time for 90 days. The color in Fig. 4 codes the values of  $\lambda$  which are measured in  $\text{days}^{-1}$ . The black “ridges” (curves of the local maxima) of the Lyapunov field are known to delineate stable manifolds of the most influential hyperbolic trajectories in the region when integrating advection equations forward in time and unstable ones when integrating them backward in time. The black “ridges” on the map in Fig. 4 delineate the corresponding unstable manifolds which are by definition the curves of maximal stretching.

Figure 4a on September 5, 2003 should be compared with Fig. 3c on the same day. Both the figures demonstrate clearly a triple vortex structure, consisting of three anticyclonic eddies, with elliptic points in their centers and two hyperbolic points between the eddies. The black “ridges” in Fig. 4a, encompassing the vortex structure, are proxies of the unstable manifolds of those hyperbolic points. It is seen in Fig. 4b on October 15, 2003, to be compared with Fig. 3d, that the topographic eddy in the NS over the Stalement Bank disappeared. Both the Lyapunov and latitudinal maps reveal clearly the same eddies in the area. The Lyapunov maps are useful to characterise quantitatively mixing in the region and to reveal stable and unstable manifolds, but they do not provide us with information about the direction of transport of water masses which is the thing we are most interested in here. On the other hand, latitudinal maps, providing such an information, are not suitable to approximate those manifolds that may be of interest in studying water mixing. Thus, the Lyapunov and latitudinal maps and synoptic maps of the other Lagrangian indicators may serve complimentary tools to monitor transport and mixing in the ocean.

The simulation performed above is supported by the Argo buoy track (no. 4900162) in Summer–Fall 2003 (Fig. 5a). That buoy was captured by the anticyclonic mesoscale eddy in the Alaskan Stream shown in Fig. 3a, then exited the

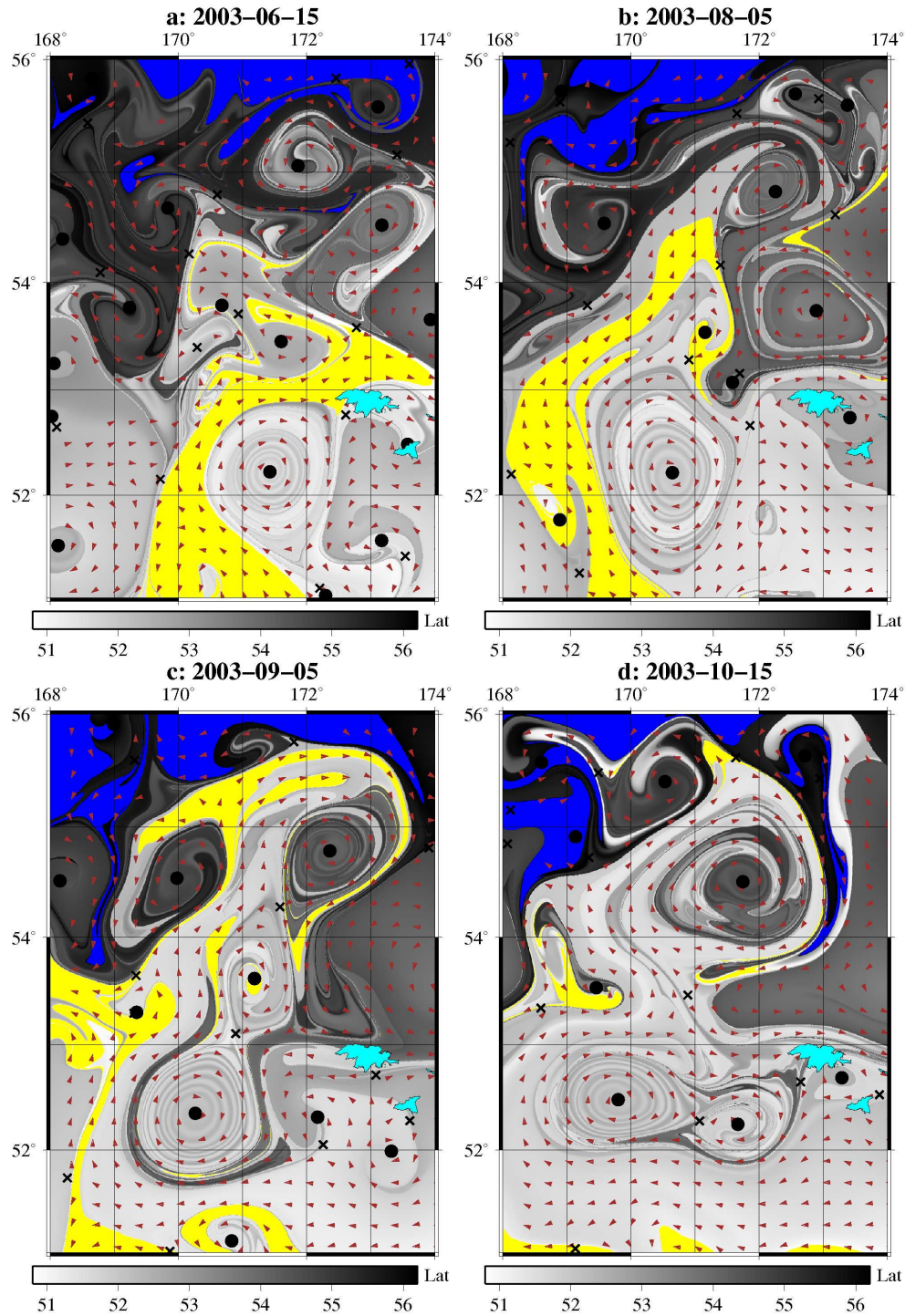


FIG. 3. Lagrangian latitudinal maps of the region in Summer-Fall of 2003 demonstrate the impact of anticyclonic eddies on the water transport across the NS. The anticyclonic mesoscale eddy is located nearby the eastern part of the strait to the south from the strait (a); the submesoscale topographic anticyclonic eddy is formed over the Stalement Bank in the strait (b); triple anticyclonic vortex structure with the mesoscale eddy to the south of the strait, the topographic eddy over the bank and the mesoscale eddy to the north of the strait controls transport across the eastern part of the strait (c); the triple vortex structure disappears opening a way to the northward transport exclusively (d). Dark grey and black colors mean that the corresponding particles came to their positions for 90 days from the latitudes to the north of the strait ( $> 54^\circ\text{N}$ ), whereas the light grey and white colors mean that the corresponding particles came from the latitudes to the south of the strait ( $< 54^\circ\text{N}$ ). (In the web version of this article “yellow” and “blue” waters crossed, respectively, the southern and the northern boundaries of the box when moving for 90 days.)



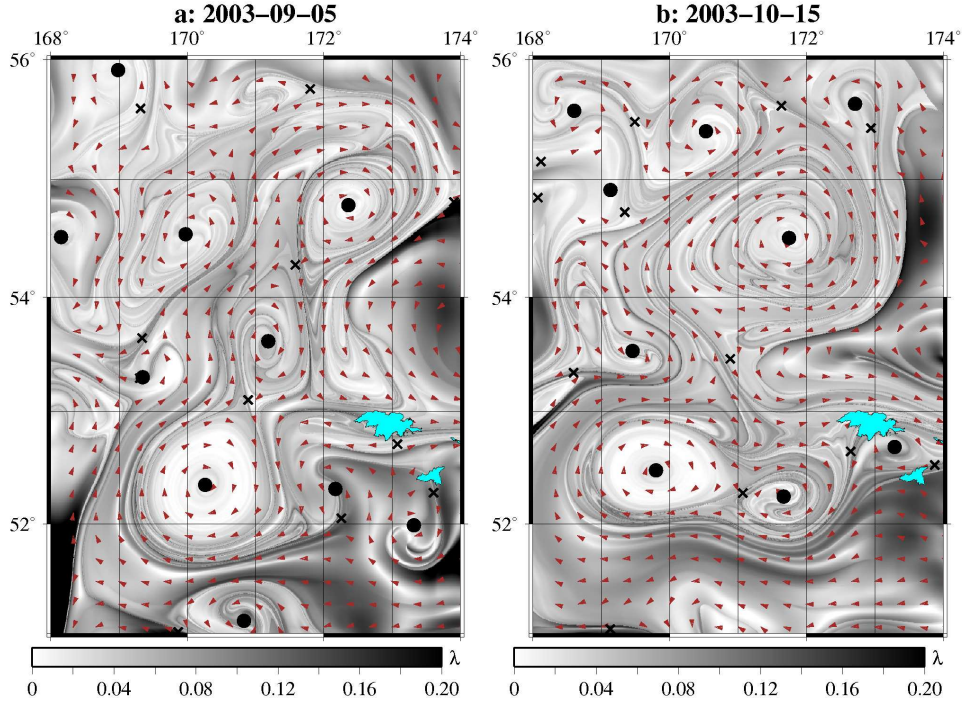


FIG. 4. Maps of the finite-time maximal Lyapunov exponents  $\lambda$  (a and b) computed on the same days as in panels c and d in Fig. 3 and under the same other conditions. Color codes the values of  $\lambda$  in  $\text{days}^{-1}$ .

eddy to the south of the NS, crossed the strait along the unstable manifold (see the grey filament encompassing that eddy on its western side in Fig. 3b). After that, it circled the anticyclonic eddy to the north of the NS (Figs. 3c and d and 4a and b) and then crossed the NS through the eastern part of the strait.

Water transport through the strait and its directions through different parts of the NS depend mainly on the hydrological situation there. By analyzing Lagrangian maps in 1993–2013, we have found four typical situations with the different number, scale and polarity of eddies to be present around and in the strait. In Fig. 6 we illustrate those four cases on the latitudinal maps which demonstrate clearly not only the eddies present in the area but the origin and history of water masses as well.

Figure 6a is an example of the situation with a mesoscale cyclonic eddy to the south of the NS ( $x_0 = 170^\circ 30'E$ ,  $y_0 = 52^\circ 15'N$ ) and a smaller scale cyclonic eddy to the north of it ( $x_0 = 170^\circ 30'E$ ,  $y_0 = 53^\circ 30'N$ ) with two elliptic points in their centers and a hyperbolic point between them. Both the eddies are clearly seen in that panel dated by August 1, 2009. It is seen that the southern cyclonic eddy enhances the flow from the Bering Sea in the western part of the NR. The ocean waters flow northward to the Bering Sea mainly through the central part of the NR (“light grey” waters). Two months later the mesoscale cyclone slightly shifted to the east (Fig. 6b on October, 1). The submesoscale anticyclonic topographic eddy was formed over the Stalement Bank in the NS practically at the same place as in August 2003 and a mesoscale anticyclonic eddy with the center around  $x_0 = 170^\circ 15'E$ ,  $y_0 = 55^\circ N$  appeared to the north of it. This vortex structure cardinally changed the direction of transport through the strait. The waters from the Pacific Ocean now flow as a narrow white (yellow in the web version) meandering jet through the eastern part of the NS along the unstable manifolds of that vortex system encompassing all the eddies. In spring 2012 the situation was changed again. The latitudinal map in Fig. 6c on April 15, 2012 shows a dipole vortex with a large anticyclonic eddy to the south of the NS ( $x_0 = 170^\circ 30'E$ ,  $y_0 = 51^\circ 30'N$ ) and a cyclonic one in the strait ( $x_0 = 170^\circ 30'E$ ,  $y_0 = 53^\circ N$ ). That dipole organizes the flow in such a way that the ocean waters (“white” and “yellow” ones in the printed and web versions, respectively) turn around both the eddies and between them blocking the flux through the NS. Spiral-like sleeves of those waters reflect the process of trapping of waters by the eddies from different latitudes for a period of integration (90 days).

The latitudinal map in Fig. 6d has been computed on September 1, 2012 demonstrating the large scale anticyclone to the south of the NS with the center around  $x_0 = 171^\circ 30'E$ ,  $y_0 = 51^\circ 30'N$  and the submesoscale topographic anticyclonic eddy over the Stalement Bank in the strait. In difference from the situation in September 2003 (Fig. 3c) there is no mesoscale anticyclone to the north of the strait in September 2012. This twin vortex structure intensifies the flux to the Bering Sea through the central part of the NS (“white” and “yellow” waters in the printed and web



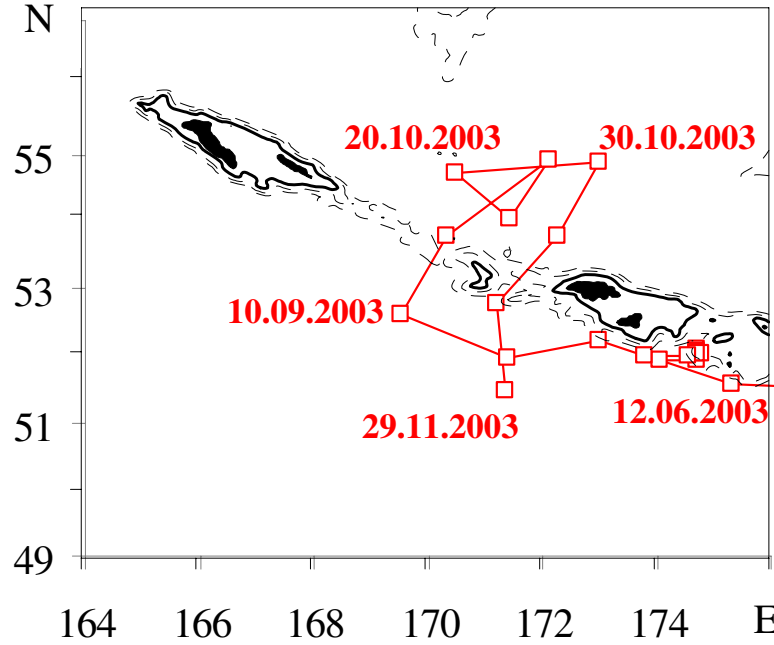


FIG. 5. Trajectory of the Argo buoy (no. 4900162) in Summer–Fall of 2003.

versions, respectively) without a significant outflow from the sea through its eastern part.

By the eddy formation and interaction we can explain the results of the current mooring measurements conducted in the NS from August 1991 until September 1992 [1]. Altimetry data, provided by [www.eddy.colorado.edu/ccar](http://www.eddy.colorado.edu/ccar), demonstrate that flow pattern observed in the NS in June–August 1992 was similar to those in July–October 2003 (Fig. 3). Interaction of the anticyclonic eddy located to the south off NS with the Stalement Bank was led to the formation of the positive SSH anomaly in the NS in June 1992. In late August 1992 this SSH anomaly moved northward into the Bering Sea and was captured by the mesoscale anticyclonic eddy to the north of NS (Fig. 3b). The formation of the positive SSH anomaly in the Stalement Bank area could result in the increased northward flow in the central part and southward flow in the eastern part of the NS. This conclusion agrees well with the current mooring observations (Reed and Stabeno [1] see their Figs. 7 and 8). In June–August 1992 subsurface northward flow was intensified in the central part of the strait (to the west of the Stalement Bank) and the flow reversed from the weak northward to the strong southward in the eastern part of the NS (to the east of the Stalement Bank). In September 1992 (when the positive SSH anomaly moved into the Bering Sea) the flow in the eastern side of the strait reversed from the southward to the northward.

Until recently, the detailed study of the impact of cyclonic eddies on the volume flux between the Bering Sea and the Pacific Ocean has not been conducted. Partly it's due to difficulties in cyclonic eddies identification by using infrared and ocean color satellite images. The Lagrangian simulation helps to shed light on that problem by computing daily latitudinal maps in the area. Lagrangian maps presented in Fig. 6 demonstrate the effect of mesoscale and submesoscale cyclonic and anticyclonic eddies on the water transport through the NS in 2009 and 2012. During April–June 2012, the central and eastern parts of the NS were under the influence of the mesoscale cyclonic eddy located to the south of the strait. The formation of the submesoscale cyclonic eddy in the central part of the NS in April forced the northward flow on the eastern side of the strait and the southward flow through the central part.

In October 2009 and September 2012, the strengthening of the mesoscale anticyclonic eddies to the north of and south of the NS led to the replacement of the submesoscale cyclone by the submesoscale anticyclone in the central part of the strait and thereby changed the flow pattern in the strait. In October 2009, the transport through central part of the strait changed its direction from the southward to the northward. During August 2012, the Alaskan Stream waters recirculated on periphery of the anticyclone to the south of the NS and did not penetrate into the strait. In September 2012, due to the appearance of a submesoscale anticyclonic eddy in the central part of the NS, the water flux was directed from the Pacific into the Bering Sea through the central part of the strait, then the flow undergone a retroflexion and it supplied into the Bering Sea on the eastern side of the NS (Fig. 6).

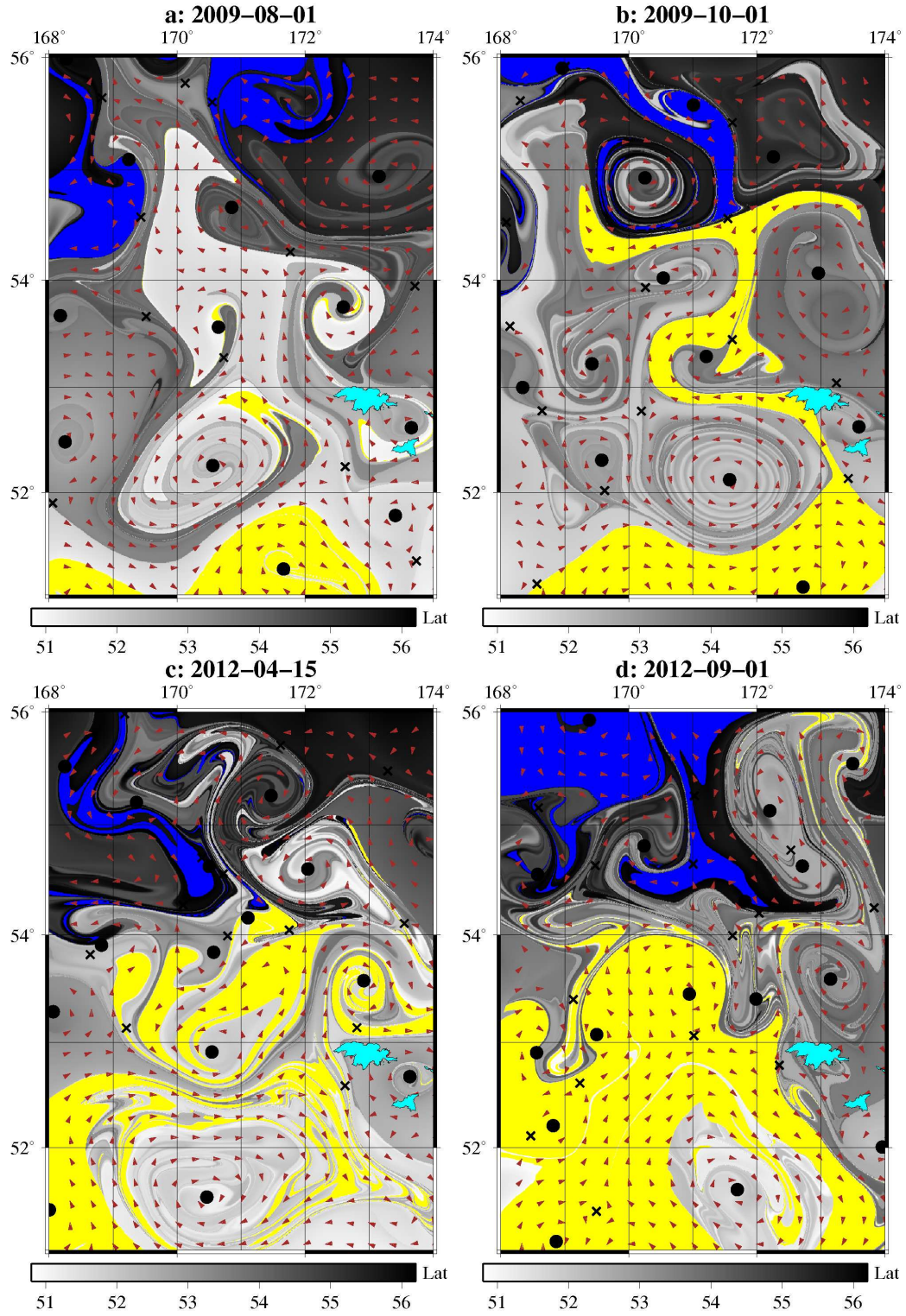


FIG. 6. Lagrangian latitudinal maps for four typical situations demonstrating the impact of cyclonic and anticyclonic eddies on the water transport across the NS. Mesoscale cyclonic eddy to the south of the NS and a smaller scale cyclonic eddy to the north (a); triple eddy structure consisting of the cyclonic mesoscale eddy, topographic anticyclonic eddy over the Stalement Bank and a mesoscale anticyclonic eddy to the north of the NS (b); the dipole vortex with the large anticyclonic eddy to the south of the NS and a cyclonic one in the strait (c); the mesoscale anticyclone to the south of the NS and the submesoscale topographic anticyclonic eddy over the Stalement Bank (d). The color legend is the same as in Fig. 3.

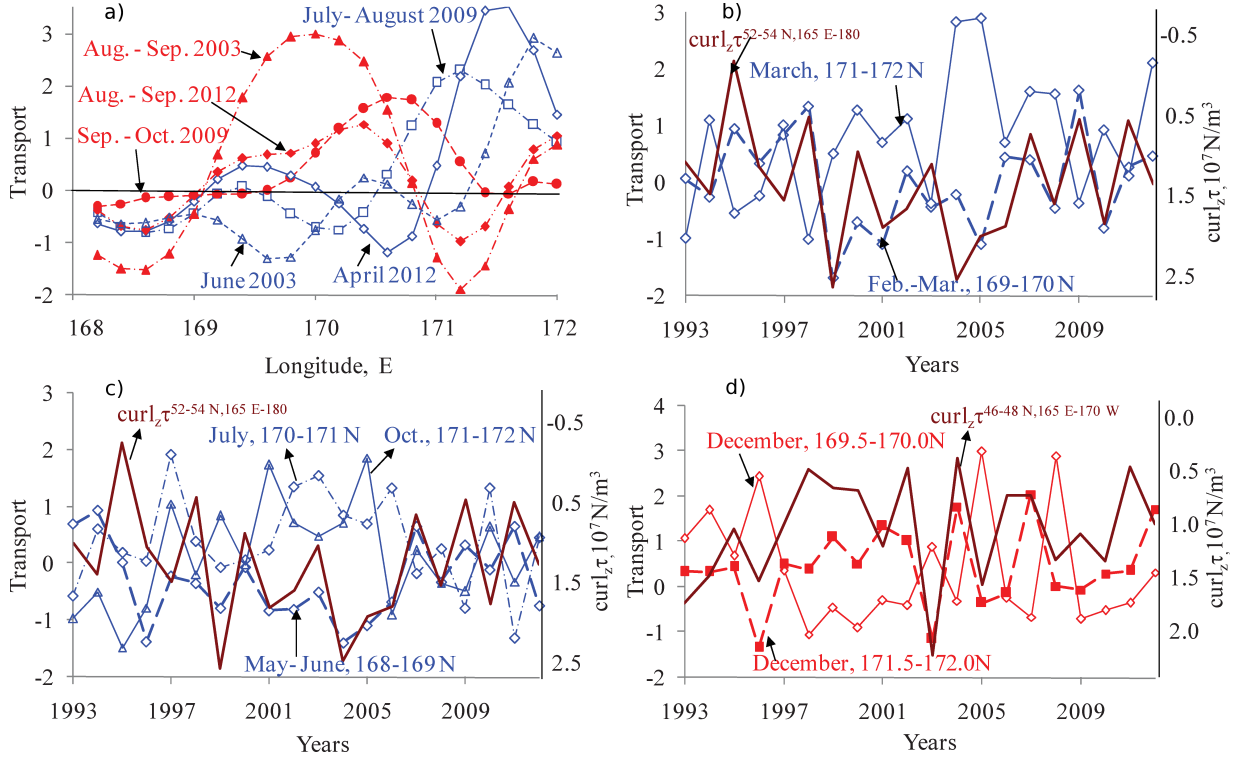


FIG. 7. Monthly averaged water transport in different parts of the NS in 2003 (June, Aug.-Sep.), 2009 (July-Aug., Sep.-Oct.) and 2012 (April, Aug.-Sep.) (a); year-to-year changes of the water transport through the NS and the wind stress curl (Nov.-Mar.) in the NS area (b, c) and central subarctic Pacific (d).

The observations from the Argo buoys provide information about the water property in the NS. Two types of water masses are observed in the strait area, relatively warm ( $> 4^\circ\text{C}$  at 50–200 m) Alaskan Stream waters and the western subarctic waters ( $< 4^\circ\text{C}$  at 50–100 m). The Alaskan Stream is a continuation of the Alaska Current originated in the NE Pacific. Western subarctic waters are supplied into the NS area on the eastern periphery of the Western Subarctic (cyclonic) Gyre. In April 2012 the water masses flowing into the Bering Sea through the eastern part of the NS was composed by the Alaskan Stream waters and western subarctic waters. In September 2012, the main source of the northward flow through the NS was the Alaskan Stream.

Fig. 7a shows the flow reversals in the central and eastern parts of the NS in 2003, 2009 and 2012. The reversals occur due to the relative positions of mesoscale eddies both to the north and to the south of the NS and the cyclonic and anticyclonic submesoscale eddies in the strait (Figs. 3, 4 and 6). In June 2003, July–August 2009 and April 2012 a submesoscale cyclone has pushed part of the Alaskan Stream into the NS, causing a northward flow on the eastern side of the strait and a southward flow in the central part of the strait. The formation of the submesoscale anticyclone during August–September 2003, September–October 2009 and August–September 2012 modified the flow through the NS, creating a strong northward flow through the central part of the strait and a southward flow on its eastern side.

### C. Relationship between the wind stress curl and the eddy intensity

The strength and position of the Aleutian Low pressure cell are main factors which determine the oceanic dynamics in the northern North Pacific. The strong Aleutian Low and positive wind-stress curl pattern over the northern North Pacific in November–March spin-up of the subarctic cyclonic gyre (see e.g. [28]). One may assume that that spin-up of the subarctic gyre results in more eddy activity on its northern boundary (Alaskan Stream region). Our results demonstrate that on the seasonal time scale the volume flux through the NS depends on wind stress curl ( $\text{curl}_z \tau = \partial \tau_y / \partial x - \partial \tau_x / \partial y$ , where  $\tau_y$  and  $\tau_x$  are respectively meridional and zonal wind stress components) in the northern North Pacific (Figs. 7b–d). Increased wind stress curl over the NS in November–March enhances the southward transport on the western side and a northward flow on the eastern side of the NS during winter and spring ( $r = -0.68$  and  $0.61$ , 1993–2012) (Figs. 7b, 7c). The cyclonic circulation is accompanied by decreased SSH in the NS

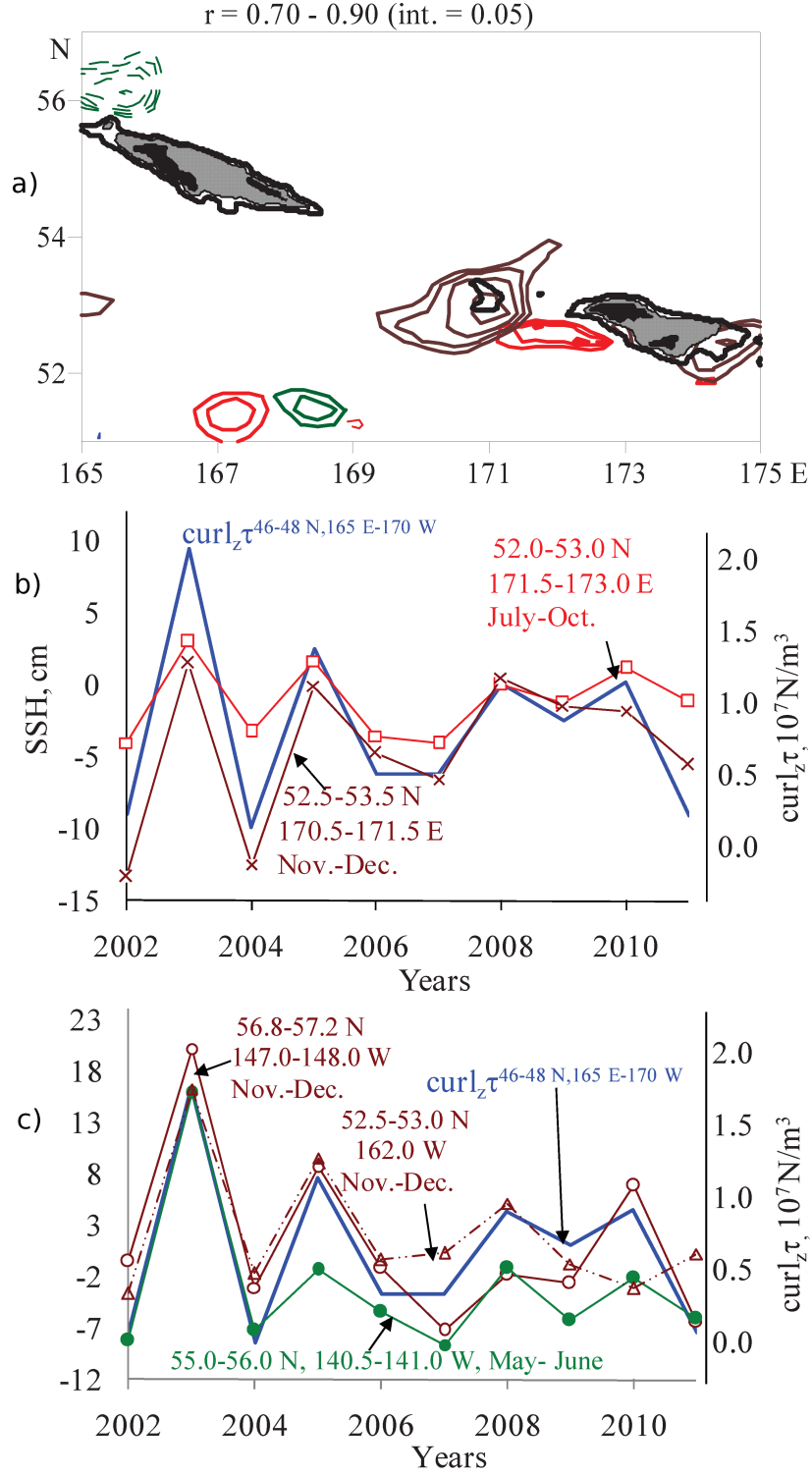


FIG. 8. Correlation coefficients between the temporal changes of the sea level in the NS area and the wind stress curl (Nov.–Mar.) in the central subarctic Pacific (a); year-to year changes of the sea level in the NS area (b) and at northern and western boundaries of the subarctic Pacific (c) and the wind stress curl (Nov.–Mar.) in the central subarctic Pacific (b–c).

area ( $r = -(0.75-0.90)$ , 2002–2012).

In addition to local forcing, our results demonstrate that the wind stress curl in the central part of the subarctic North Pacific ( $46^\circ\text{N}$ – $48^\circ\text{N}$ ,  $165^\circ\text{E}$ – $170^\circ\text{E}$ ) determines the year-to-year changes in water transport through the NS

during fall (Fig. 7d). Large positive wind stress curl in the subarctic Pacific corresponds to increased northward volume flux in the central part of the NS ( $r = 0.66$ ) and vice versa for the eastern side of the strait ( $r = -0.62$ ). The flow pattern in the NS during fall (October–December) is determined by the strength of the anticyclonic eddy in the strait area. Analysis of the SSH time series at the northern boundary of the subarctic gyre (the Alaskan Stream and the Alaska Current) revealed that the year-to-year changes of the SSH in the anticyclonic eddies are related to the wind stress curl ( $r = 0.85$ – $0.89$ , 2002–2012) (Figs. 8a–c). Spin up of the subarctic cyclonic gyre forced by the wind stress curl intensifies the boundary currents, increases the sea level at the gyre boundaries and probably enhances the anticyclonic eddy activity in the Alaskan Stream area. Our conclusions are supported by the results of Ladd et al. [29]. They indicated that the anticyclonic eddy activity along the eastern shelf-break of the Bering Sea during the spring months is negatively correlated with the North Pacific Index, a measure of the strength of the Aleutian Low in November–March. The proposed mechanisms for the creation of anticyclonic eddies include instabilities and the interaction of the boundary currents with topographic features.

#### IV. CONCLUSION

The Lagrangian approach, based on the AVISO surface velocity field, is applied to study temporal and spatial variations of the transport between the Bering Sea and the North Pacific. Our results demonstrate that the eddy activity in the vicinity of the Near Strait has a strong impact on the flow through the strait. Generation of anticyclonic and cyclonic submesoscale eddies in the Near Strait leads to the flow reversals in central and eastern parts of the strait and westward (or eastward) shift in the velocity core. In June 2003, July–August 2009 and April 2012 a submesoscale cyclone has pushed part of the Alaskan Stream into the Near Strait, causing a northward flow on the eastern side of the strait and a southward flow in its central part. The formation of the submesoscale anticyclone during August–September 2003, September–October 2009 and August–September 2012 modified the flow through the Near Strait creating a strong northward flow through the central part and southward flow on the eastern side.

On the interannual time scale, significant positive correlation ( $r = 0.72$ ) is diagnosed between the Near Strait transport and the wind stress in winter. Increased southward component of the wind stress decreases the northward water transport through the strait. Positive wind stress curl over the strait area in winter–spring generates the cyclonic circulation and thereby enhances the southward flow in the western part ( $r = -0.68$ ) and northward flow in the eastern part ( $r = 0.61$ ) of the Near Strait. During fall, the wind stress curl over the northern North Pacific (November–March) are responsible for eddy activity in the Alaskan Stream area and the flux pattern in the Near Strait.

#### ACKNOWLEDGMENTS

This work was supported by the Russian Foundation for Basic Research (project nos. 11–05–98542, 12–05–00452, and 13–05–00099). The altimeter products were distributed by AVISO with support from CNES.

- 
- [1] R. K. Reed and P. J. Stabeno, *Journal of Marine Research* **51**, 515 (1993).
  - [2] T. Ezer and L.-Y. Oey, *Ocean Dynamics* **63**, 243 (2013).
  - [3] J. Clement Kinney and W. Maslowski, *Deep Sea Research Part I: Oceanographic Research Papers* **66**, 11 (2012).
  - [4] G. Panteleev, M. Yaremchuk, V. Luchin, D. Nechaev, and T. Kukuchi, *Journal of Oceanography* **68**, 485 (2012).
  - [5] P. J. Stabeno and R. K. Reed, *Geophysical Research Letters* **19**, 1671 (1992).
  - [6] S. R. Okkonen, *Journal of Geophysical Research* **101**, 8839 (1996).
  - [7] P. J. Stabeno, J. D. Schumacher, and K. Ohtani, in *Dynamics of the Bering Sea: A Summary of Physical, Chemical, and Biological Characteristics, and a Synopsis of Research on the Bering Sea*, Alaska Sea Grant College Program report, Vol. 99, edited by T. Loughlin and K. Ohtani (University of Alaska Sea Grant, 1999) pp. 1–28.
  - [8] G. Haller, *Physics of Fluids* **14**, 1851 (2002).
  - [9] E. R. Abraham and M. M. Bowen, *Chaos: An Interdisciplinary Journal of Nonlinear Science* **12**, 373 (2002).
  - [10] F. d'Ovidio, V. Fernández, E. Hernández-García, and C. López, *Geophys. Res. Lett.* **31**, L17203 (2004).
  - [11] K. V. Koshel and S. V. Prants, *Physics Uspekhi* **49**, 1151 (2006).
  - [12] M. J. Olascoaga, I. I. Rypina, M. G. Brown, F. J. Beron-Vera, H. Koçak, L. E. Brand, G. R. Halliwell, and L. K. Shay, *Geophys. Res. Lett.* **33**, L22603 (2006).
  - [13] Y. Lehn, F. d'Ovidio, M. Lévy, and E. Heifetz, *J. Geophys. Res.* **112**, C08005 (2007).
  - [14] F. J. Beron-Vera, M. J. Olascoaga, and G. J. Goni, *Geophys. Res. Lett.* **35**, L12603 (2008).
  - [15] C. S. Harrison and G. A. Glatzmaier, *Geophys. Astrophys. Fluid Dyn.* **106**, 22 (2012).

- [16] S. Prants, M. Budyansky, V. Ponomarev, and M. Uleysky, *Ocean Modelling* **38**, 114 (2011).
- [17] S. R. Keating, K. S. Smith, and P. R. Kramer, *J. Phys. Oceanogr.* **41**, 1512 (2011).
- [18] I. Hernández-Carrasco, C. López, E. Hernández-García, and A. Turiel, *Ocean Modelling* **36**, 208 (2011).
- [19] F. Huhn, A. von Kameke, V. Pérez-Muñuzuri, M. J. Olascoaga, and F. J. Beron-Vera, *Geophys. Res. Lett.* **39**, L06602 (2012), 10.1029/2012GL051246.
- [20] S. V. Prants, *Physica Scripta* **87**, 038115 (2013).
- [21] S. V. Prants, V. I. Ponomarev, M. V. Budyansky, M. Y. Uleysky, and P. A. Fayman, *Izvestiya, Atmospheric and Oceanic Physics* **49**, 82 (2013).
- [22] R. M. Samelson and S. Wiggins, *Lagrangian Transport in Geophysical Jets and Waves: The Dynamical Systems Approach (Interdisciplinary Applied Mathematics)* (Springer, 2006).
- [23] H. Aref, *Journal of Fluid Mechanics* **143**, 1 (1984).
- [24] S. V. Prants, M. Y. Uleysky, and M. V. Budyansky, *Doklady Earth Sciences* **439**, 1179 (2011).
- [25] E. Kalnay, M. Kanamitsu, R. Kistler, W. Collins, D. Deaven, L. Gandin, M. Iredell, S. Saha, G. White, J. Woollen, and et al., *Bulletin of the American Meteorological Society* **77**, 437 (1996).
- [26] F. d'Ovidio, J. Isern-Fontanet, C. López, E. Hernández-García, and E. García-Ladona, *Deep Sea Research Part I: Oceanographic Research Papers* **56**, 15 (2009).
- [27] J. M. Ottino, *The Kinematics of Mixing: Stretching, Chaos, and Transport* (Cambridge University Press, Cambridge, U.K., 1989).
- [28] Y. Ishi, *Geophysical Research Letters* **32** (2005), 10.1029/2004GL022330.
- [29] C. Ladd, P. J. Staben, and J. E. O'Hern, *Deep Sea Research Part I: Oceanographic Research Papers* **66**, 67 (2012).